Novel Pentagonal MgX_2 (X=O, S, Se, Te) Monolayers: Promising Photocatalysts for Overall Water Splitting and CO_2 Reduction

Zhanyao Xu [a,b,1], Sajid Ur Rehman[a,b,1], Yuan Xu[a], Haris Habib[c], Zeeshan Tariq[a,b], Hafiz Muhammad Naeem Ullah[a,b], Yang Wang [a,b]*, Chuanbo Li[a,b]*,Xiaoming Zhang

[a] School of Science, Minzu University of China, Beijing 100081, China
[b] Optoelectronics Research Center, Minzu University of China, Beijing 100081, People's Republic of China
[c] Henan Key Laboratory of Quantum Materials and Quantum Energy, School of Future Technology, Henan University, Kaifeng 475004, China

[1]Both Authors contributed equally.

*Corresponding Authors: yangwang@muc.edu.cn; cbli@muc.edu.cn

In the original calculation of carrier mobility for MgX_2 (X = O, S, Se, Te), the values of certain parameters in Formula (4) need to be obtained by fitting curves. Panels (a) and (c) of Figures S1, S2, S3, and S4 present the fitting curves for the elastic modulus constant C_{2D} of MgX_2 (X = O, S, Se, Te) along the armchair and zigzag directions, respectively. The data points on these curves represent the calculated free energy values under strains ranging from -2% to +2%. The quadratic coefficient obtained from the fitting corresponds to the value of $[\partial^2 E/\partial(\Delta l/l_0)^2]$ in the formula $C_{2D} = 2[\partial^2 E/\partial(\Delta l/l_0)^2]/S_0$.

Panels (b) and (d) of Figures S1, S2, S3, and S4 present the fitting curves for the deformation potential constant E_1 of MgX_2 (X = O, S, Se, Te) along the armchair and zigzag directions, respectively. The data points on these curves represent the calculated values of VBM-Vac and CBM-Vac under strains ranging from -2% to +2%. The slope obtained from the fitting directly provides the value of E_1 used in Formula

(4) $\mu_{2D} = (e\hbar^3 C_{2D})/(K_B T m^* m_d (E_1)^2)$. Specifically, these slope values correspond to the entries under the "DP potential (eV/strain) — $E_{d,x}$" column in Table IV.

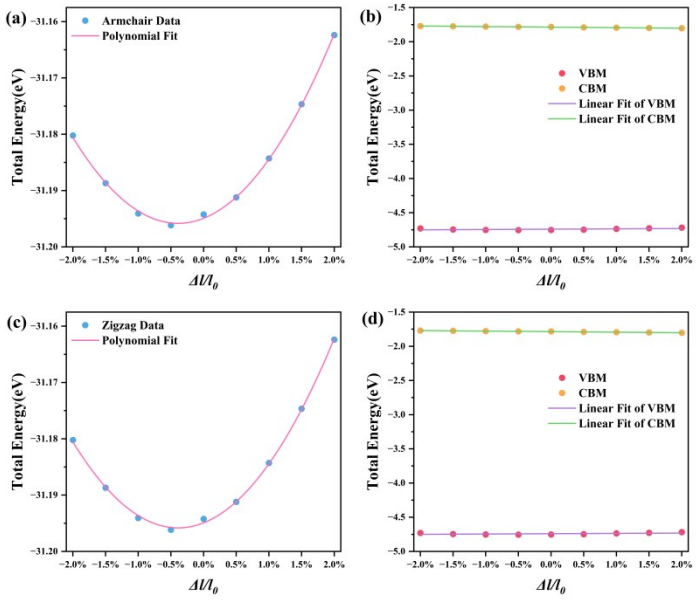

Figure S1. For MgO_2 in the Armchair direction: **(a)** fitting curve of elastic modulus constants $[\partial^2 E/\partial(\Delta l/l_0)^2]$ and **(b)** fitting curve of deformation potential constant E_1; and in the Zigzag direction: **(c)** fitting curve of elastic modulus constants $[\partial^2 E/\partial(\Delta l/l_0)^2]$ and **(d)** fitting curve of deformation potential constant E_1.

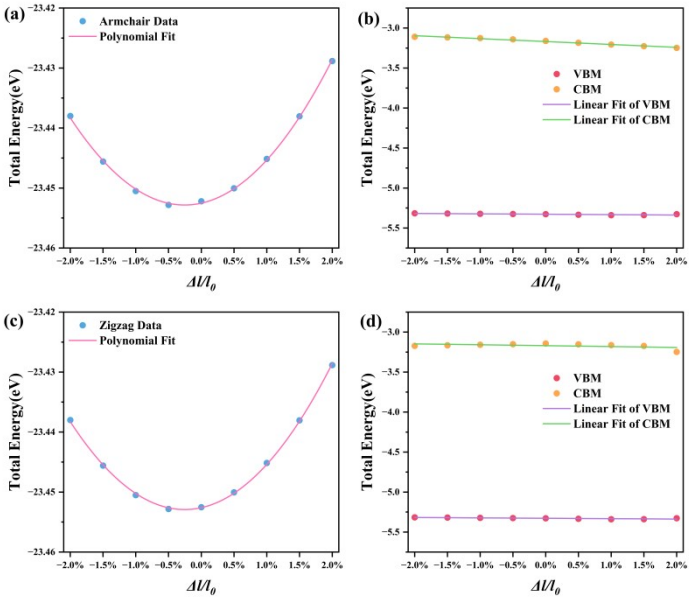

Figure S2. For MgS_2 in the Armchair direction: **(a)** fitting curve of elastic modulus

constants $[\partial^2 E/\partial(\Delta l/l_0)^2]$ and **(b)** fitting curve of deformation potential constant E_1; and in the Zigzag direction: **(c)** fitting curve of elastic modulus constants $[\partial^2 E/\partial(\Delta l/l_0)^2]$ and **(d)** fitting curve of deformation potential constant E_1.

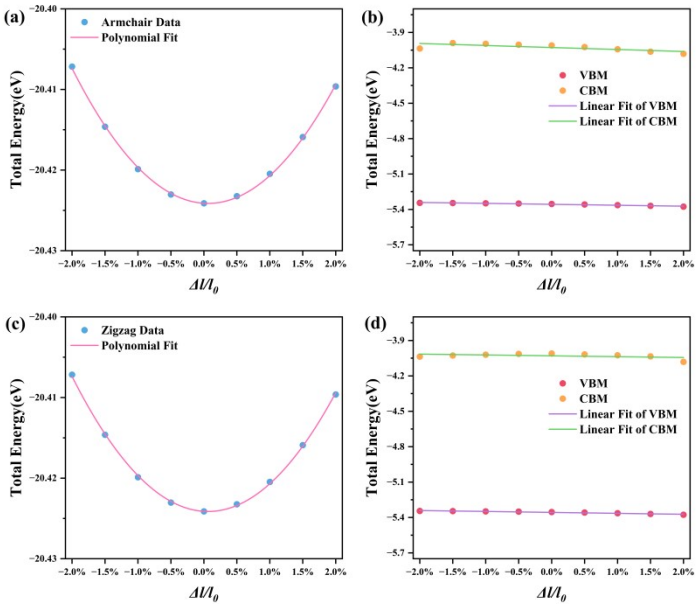

Figure S3. For $MgSe_2$ in the Armchair direction: **(a)** fitting curve of elastic modulus constants $[\partial^2 E/\partial(\Delta l/l_0)^2]$ and **(b)** fitting curve of deformation potential constant E_1; and in the Zigzag direction: **(c)** fitting curve of elastic modulus constants $[\partial^2 E/\partial(\Delta l/l_0)^2]$ and **(d)** fitting curve of deformation potential constant E_1.

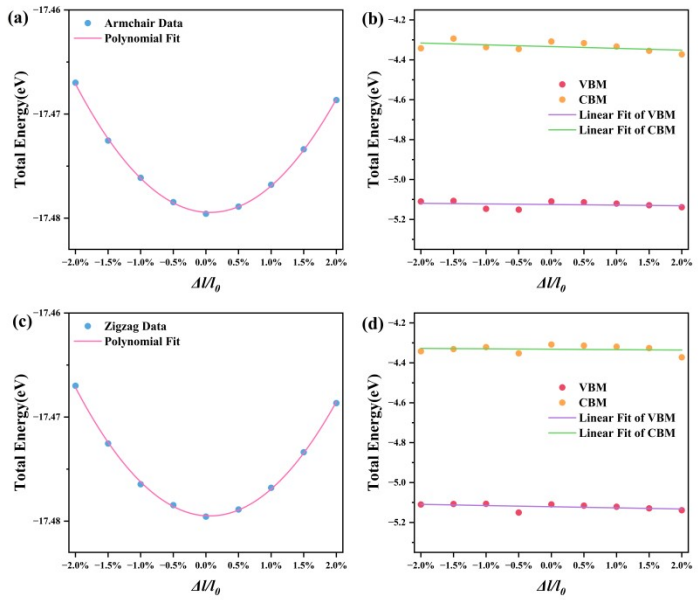

Figure S4. For $MgTe_2$ in the Armchair direction: **(a)** fitting curve of elastic modulus

constants $[\partial^2 E/\partial(\Delta l/l_0)^2]$ and **(b)** fitting curve of deformation potential constant E_1; and in the Zigzag direction: **(c)** fitting curve of elastic modulus constants $[\partial^2 E/\partial(\Delta l/l_0)^2]$ and **(d)** fitting curve of deformation potential constant E_1.

Visualizing the optimized adsorption configurations can significantly enhance the clarity and accessibility of catalytic analysis. Therefore, we have supplemented this manuscript with schematic diagrams of the optimized adsorption configurations for each intermediate state in the calculation of Gibbs free energy for HER, OER, and CO_2RR on MgX_2 (X = O, S, Se, Te), as shown in Figures S5, S6, S7, S8, and S9.

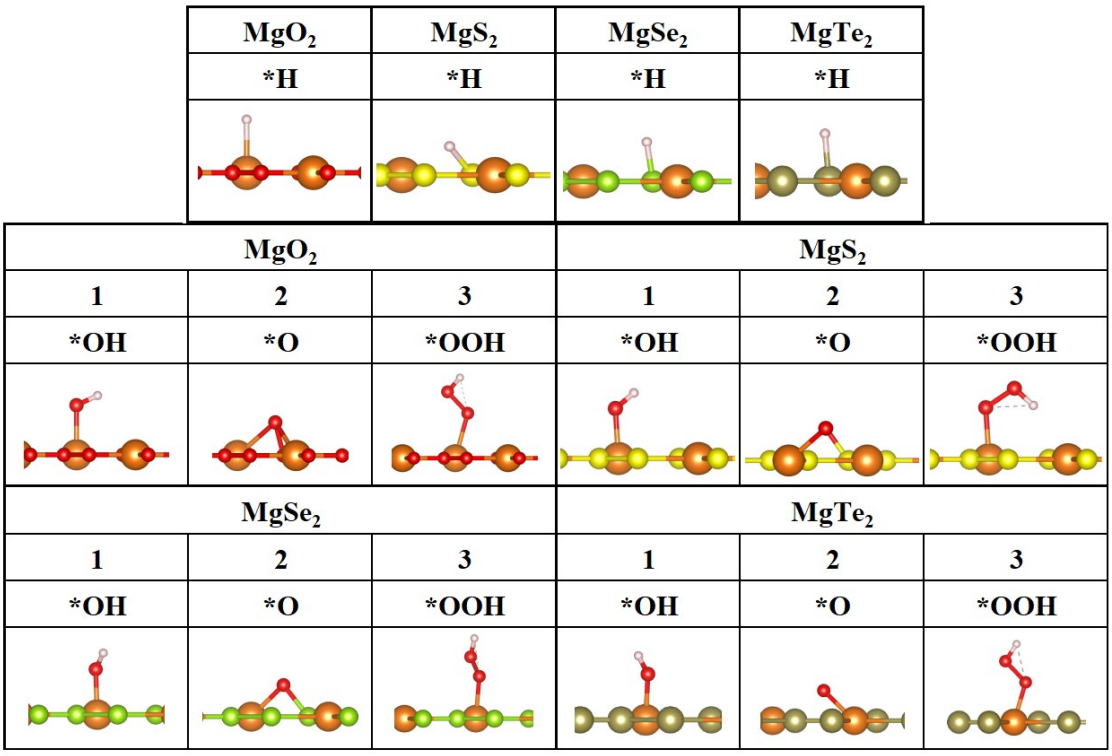

Figure S5. Important reaction intermediates in electrochemical HER and OER process on pentagonal MgX_2 (X=O,S,Se,Te) monolayers.

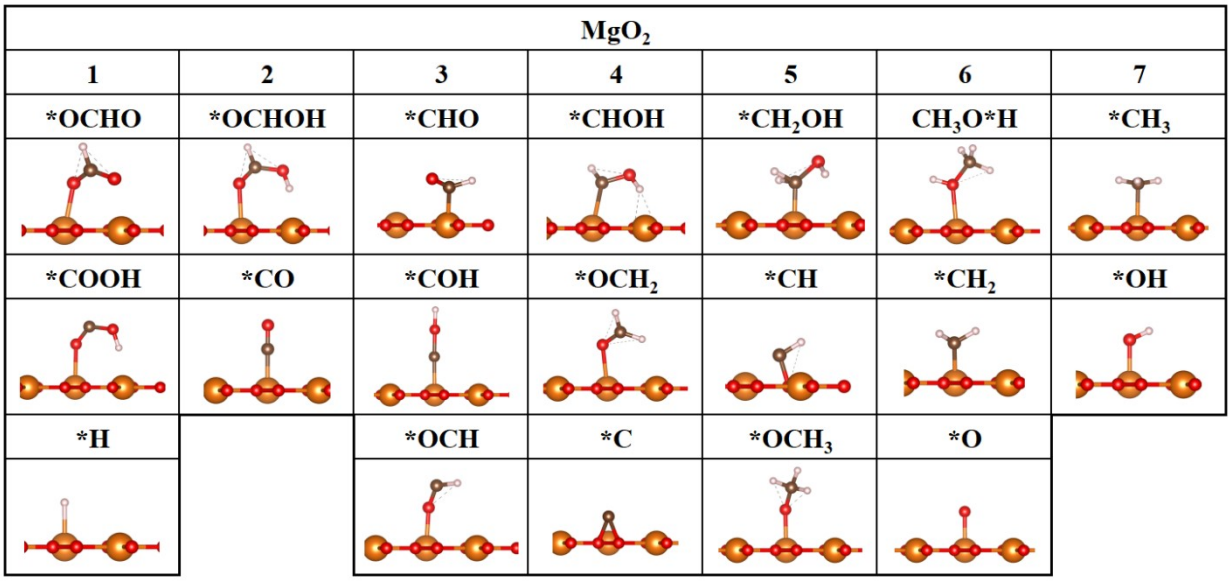

Figure S6. Important reaction intermediates in electrochemical CO_2RR process on pentagonal MgO_2 monolayer.

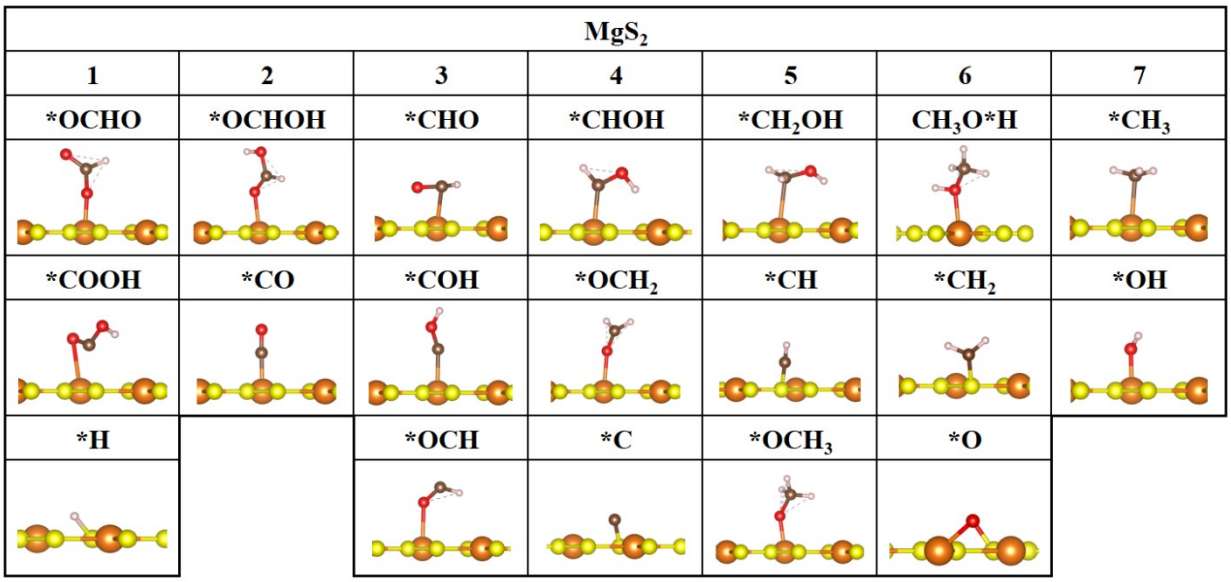

Figure S7. Important reaction intermediates in electrochemical CO_2RR process on pentagonal MgS_2 monolayer.

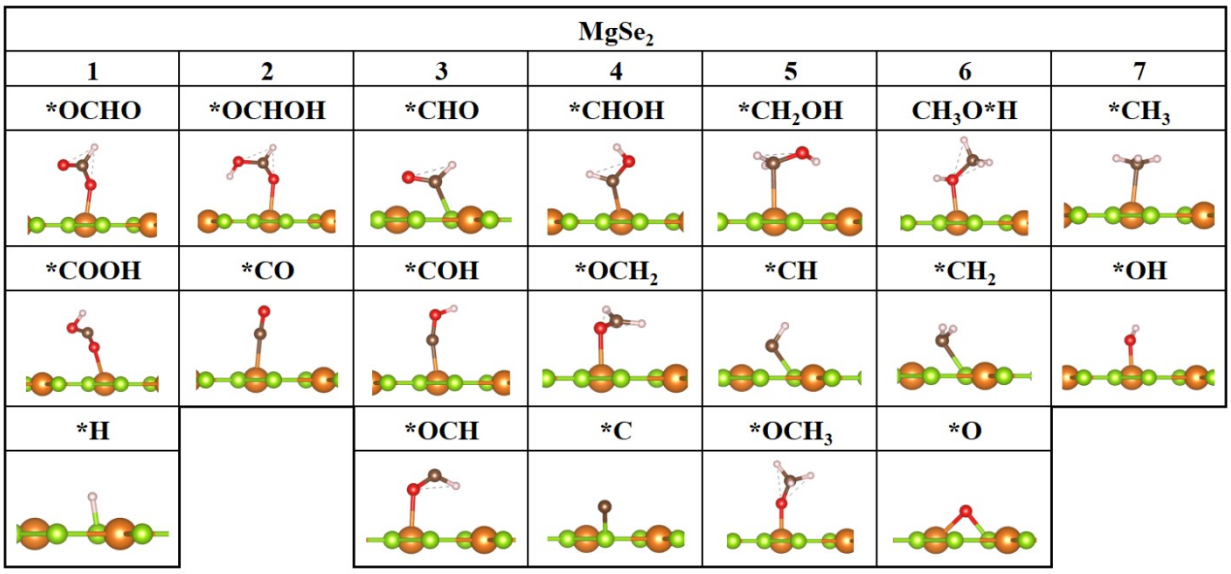

Figure S8. Important reaction intermediates in electrochemical CO_2RR process on pentagonal $MgSe_2$ monolayer.

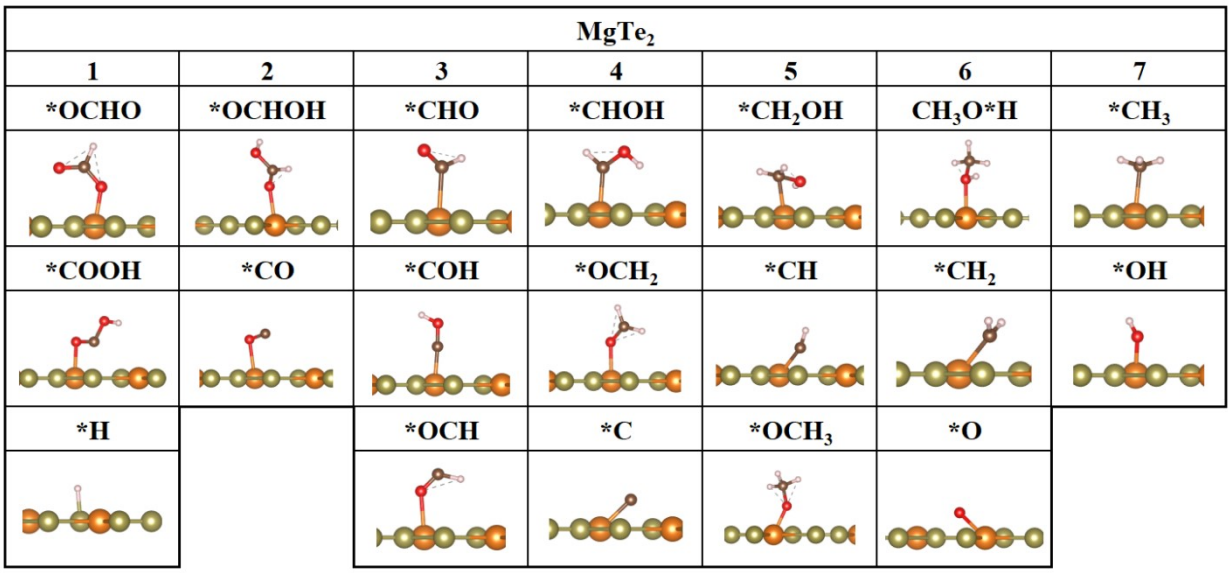

Figure S9. Important reaction intermediates in electrochemical CO_2RR process on pentagonal $MgTe_2$ monolayer.

In Figure 8, we have clearly labeled the Gibbs free energy values for the key intermediates. Furthermore, we have provided a supplementary table (Table S1) that lists the contributions of electronic energy (E_{DFT}), zero-point energy (ZPE), and

entropy correction (TΔS) for each adsorbed species and reaction step. This comprehensive presentation ensures complete transparency of the thermodynamic data underlying the Gibbs free energy profile and reinforces our conclusion that, among the studied monolayer materials, $MgTe_2$ provides the most favorable pathway for CO_2 conversion.

Table S1. Calculated total energy (E_{DFT}/eV), zero-point energies (ZPE/eV), entropy corrections (TΔS/eV,T/298.15 K) and Gibbs free energy (ΔG/eV) for the adsorption species on Penta-$MgTe_2$ monolayers.

Species	E_{DFT}(eV)	ZPE(eV)	TΔS(eV)
***COOH**	-42.670067	0.593543	0.185732
***OCHO**	-43.506857	0.582593	0.206176
***H**	-19.756442	0.171113	0.028591
***OCHOH**	-47.744637	0.915414	0.299293
***CO**	-32.362707	0.142535	0.300828
***COH**	-33.275609	0.393635	0.182787
***CHO**	-35.034016	0.411112	0.170922
***OCH**	-34.592688	0.381413	0.231484
***CHOH**	-39.010112	0.767493	0.117539
***C**	-21.255705	0.061944	0.064015
***OCH_2**	-40.233406	0.754165	0.173618
***CH_2OH**	-42.530141	1.019496	0.167434
***CH**	-26.794366	0.333606	0.093334
***OCH_3**	-43.608901	1.059379	0.205801
***CH_3O*H**	-48.551392	1.401553	0.211886
***CH_2**	-32.200771	0.648931	0.072547
***O**	-23.547425	0.070404	0.054565
***CH_3**	-36.073398	0.902907	0.181185
***OH**	-27.424995	0.437998	0.534553

Explicitly listing the energy barrier values for each key elementary step in the CO_2 reduction pathway will help enhance the clarity and completeness of the discussion. To this end, we have supplemented Table S2 with the calculated energy barrier values ($\Delta E^{\ddagger}$) for the key steps in the reduction of CO_2 to CH_4 on the $MgTe_2$ monolayer. The data confirm that the energy barrier for the rate-determining step remains at a relatively low level, which supports our conclusion regarding the favorable performance of $MgTe_2$ in CO_2RR.

Table S2. Energy barrier values of key steps in Penta-$MgTe_2$.

key step	$\Delta E^{\ddagger}$(eV)
$*+CO_2 \rightarrow *OCHO$	0.88
$*OCHO \rightarrow *OCHOH$	-0.55
$*OCHOH \rightarrow *CHO$	1.54
$*CHO \rightarrow *CHOH$	-0.12
$*CHO \rightarrow *OCH_2$	-1.42
$*CHOH \rightarrow *CH_2OH$	0.12
$*OCH_2 \rightarrow *OCH_3$	0.35
$*CH_2OH \rightarrow CH_3O*H$	-2.24
$*OCH_3 \rightarrow CH_3O*H$	-1.17
$*OCH_3 \rightarrow *O$	-0.77
$*O \rightarrow *OH$	-0.54

$CH_3O^*H \rightarrow {}^*OH$	-0.14